


RESEARCH ARTICLE

An ETS-NOCV-based computational strategies for the characterization of concerted transition states involving CO₂

Diego Sorbelli¹ | Paola Belanzoni^{1,2} | Leonardo Belpassi² | Ji-Woong Lee^{3,4} | Gianluca Ciancaleoni^{5,6} 

¹Department of Chemistry, Biology and Biotechnology, University of Perugia, Perugia, I-06123, Italy

²CNR Institute of Chemical Science and Technologies “Giulio Natta” (CNR-SCITEC), c/o Department of Chemistry, Biology and Biotechnology, University of Perugia, Perugia, I-06123, Italy

³Department of Chemistry, University of Copenhagen, Copenhagen, Ø 2100, Denmark

⁴Nanoscience Center, University of Copenhagen, Copenhagen, Ø 2100, Denmark

⁵Department of Chemistry and Industrial Chemistry, University of Pisa, Pisa, I-56124, Italy

⁶CIRCC, Bari, Italy

Correspondence

Gianluca Ciancaleoni, Department of Chemistry and Industrial Chemistry, University of Pisa, via G. Moruzzi 13, I-56124 Pisa, Italy. Email: gianluca.ciancaleoni@unipi.it

Abstract

Due to the presence of both a slightly acidic carbon and a slightly basic oxygen, carbon dioxide is often involved in concerted transition states (TSs) with two (or more) different molecular events interlaced in the same step. The possibility of isolating and quantitatively evaluating each molecular event would be important to characterize and understand the reaction mechanism in depth. This could be done, in principle, by measuring the relevant distances in the optimized TS, but often distances are not accurate enough, especially in the presence of many simultaneous processes. Here, we have applied the Extended Transition State-Natural Orbital for Chemical Valence-method (ETS-NOCV), also in combination with the Activation Strain Model (ASM) and Energy Decomposition Analysis (EDA), to separate and quantify these molecular events at the TS of both organometallic and organic reactions. For the former, we chose the decomposition of formic acid to CO₂ by an iridium catalyst, and for the latter, a CO₂-mediated transamidation and its chemical variations (hydro- and aminolysis of an ester) as case studies. We demonstrate that the one-to-one mapping between the “molecular events” and the ETS-NOCV components is maintained along the entire lowest energy path connecting reactants and products around the TS, thus enabling a detailed picture on the relative importance of each interacting component. The methodology proposed here provides valuable insights into the effect of different chemical substituents on the reaction mechanism and promises to be generally applicable for any concerted TSs.

KEYWORDS

bond analysis, carbon dioxide, density functional theory, energy decomposition analysis, reaction mechanism

1 | INTRODUCTION

Carbon dioxide has always received great attention from chemical research, but more than ever in the last years. Indeed, there is

currently the urgency to reduce its concentration in the atmosphere (290 ppm in the pre-industrial age, reached recently a new record of 421 ppm in April 2021¹) and this generated a huge numbers of studies, both experimental and theoretical, devoted to explore the

This is an open access article under the terms of the Creative Commons Attribution-NonCommercial-NoDerivs License, which permits use and distribution in any medium, provided the original work is properly cited, the use is non-commercial and no modifications or adaptations are made.

© 2022 The Authors. *Journal of Computational Chemistry* published by Wiley Periodicals LLC.

absorption, storage and/or transformation of carbon dioxide into valuable chemicals from flue gases, directly from the atmosphere or by photocatalysis.^{2–4}

From the chemical point of view, CO₂ is quite stable ($\Delta H_f^0 = -94.0$ kcal/mol⁵), reactive in the presence of bases (amines, hydroxide ions, hydrides...), but also capable of interaction with Lewis acids (acidic sites⁶ or polarized halogens⁷). This amphoteric behavior is due to the polarization of the two C=O bonds, which originates a slightly acidic carbon and a slightly basic oxygen. The coexistence of these two sites in many reactions leads to concerted transition states (TSs), in which the carbon and the oxygen are involved in different interactions and separated molecular events.

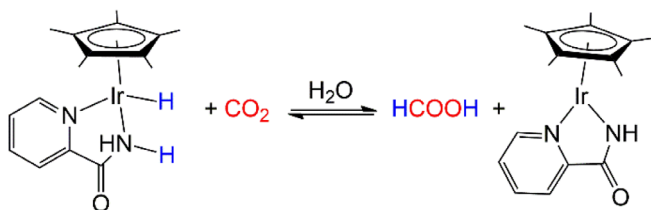
For instance, this is true for the mechanism of CO₂ activation by Frustrated Lewis Pairs (FLPs),⁸ in which the Lewis acid and the Lewis base attack the oxygen and carbon of CO₂ in a single step (even if in some case the mechanism is significantly asynchronous that becomes stepwise⁹), for example, hydration of CO₂ to carbonic acid¹⁰ and related species,¹¹ hydrosilylation of CO₂ catalyzed by metal complexes¹² and hydrogenation of CO₂ by B₃N₃H₂ compound.¹³

We encountered a concerted TS in the decomposition of formic acid to CO₂ catalyzed by a 16e iridium bifunctional complex.¹⁴ In fact, formic acid interacts at the same time with the metal vacancy and the amido moiety, donating one hydride and one proton in a concerted way and liberating CO₂. In principle, the same mechanism could be active for the reverse reaction, that is the synthesis of formic acid from CO₂ and the 18e iridium hydride complex (Scheme 1).

In a different research line, we discovered that CO₂ can also act as a catalyst for the transamidation reaction, taking advantage of its amphoteric nature.¹⁵ Indeed, the carbon atom of the CO₂ can form a covalent bond with the carbonyl oxygen of the amide, making the carbon more electrophilic, while the oxygen of CO₂ can abstract a proton from a primary/secondary amine, in a concerted or stepwise way, making the incoming nucleophile stronger (Scheme 2).

Based on the general importance of concerted TSs in the chemistry of CO₂, we tried to better characterize them, in terms of ratio between the two (or more) concerted molecular events. Obviously, distances in the TS can give insights on which molecular event is more advanced, but when a TS is particularly complex (as in the cases studied here involving three molecular events), an analysis based exclusively on distances may not be totally reliable.

As the problem concerns the decomposition and quantitative characterization of two different interactions, a possible solution can



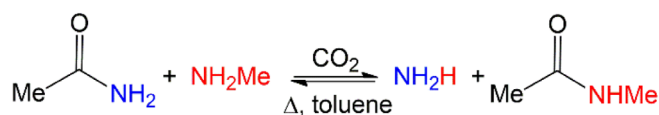
SCHEME 1 Hydrogenation of CO₂ and the reverse reaction by a bifunctional iridium hydride complex

be given by the Energy Decomposition Analysis (EDA)^{16,17} and the Extended Transition State-Natural Orbital for Chemical Valence (ETS-NOCV)^{18–20} analysis, which recently demonstrated to be a useful tool for the bond analysis of complex adducts,^{21,22} as those held together by both halogen and hydrogen bonds,²³ characterization of donation and back-donation in metal–ligand interactions^{18,24–26} and for giving insights into the recently-coined spodium bond.²⁷ While the EDA decomposes the interaction between two fragments (ΔE_{int}) into different contributions (mainly related to electrostatics, Pauli repulsion and orbital mixing), the ETS-NOCV focuses only on the orbital term, by decomposing it into chemically meaningful contributions. Although EDA and ETS-NOCV have been already used to characterize reaction paths,^{17,28–30} including the CO₂ insertion into a gold-alumanyl complex,³¹ for concerted TSs there are less examples^{32–37} and most of them deals with two-body reactions and simpler TSs, as in the case of the cycloaddition, where basically only one geometrical parameter is relevant.

To this aim, the recent Activation Strain Model (ASM) analyzes how the energy contributions change along a reaction path,^{38–41} giving precious information on the most relevant factors that govern a path. Indeed, the adduct is fragmented and the relative energy of the adduct is decomposed into two contributions: the energy needed to deform the reactants from their relaxed geometry to the geometry needed to react (ΔE_{dist}) and the actual interaction energy between the so-prepared fragments (ΔE_{int}). Plotting ΔE_{dist} and ΔE_{int} along the reaction path determines whether the reaction is strain- or interaction-driven. That is, whether the stabilizing interaction between distorted fragments is able to balance the penalty arising from the distortion of the reactants.

Here, we report our analysis for the three-body cases as illustrated in Schemes 1 and 2: the reaction between an iridium hydride complex and CO₂ to give formic acid and the CO₂-promoted transamidation reaction and its chemical variants (amino- and hydrolysis of esters). In these cases the TSs are particularly complex, involving three bodies and two or three concerted chemical events. Even in these unfavorable conditions, we show how the ETS-NOCV analysis can give interesting and chemically-relevant information regarding the nature and extent of the orbital contribution changes along the reaction pathways, where the stabilizing interaction is a fundamental contribution.

About this, we also show that the Intrinsic Reaction Coordinate (IRC) approach cannot be used to analyze the reaction pathways under study, as it is not safe with very complex TSs.^{39,40,42} On the contrary, the construction of a bidimensional cut of the Potential Energy Surface (PES) through the choice of two geometrical parameters is a more reliable and customizable strategy. Importantly, this



SCHEME 2 CO₂-promoted model transamidation reaction

choice is not arbitrary, but is dictated by the results of the ETS-NOCV analysis of the TS, which already indicates the most important contributions.

For both organometallic and organic reactions, the effect of the substituents on the reaction path and the characterization of the TS will be discussed. The results demonstrate that our combined approach provides valuable insights into the effect of chemical variations of the reactants (fluorination, variation of the nucleophile...).

2 | RESULTS AND DISCUSSION

2.1 | Iridium-catalyzed CO₂ activation

We first analyze the reaction between an iridium hydride species and CO₂ giving formic acid and a 16 electrons iridium complex as products (Scheme 1).¹⁴ Two reactant complexes (**RC_{NH}** and **RC_{CO}**) can be optimized, in both cases consisting of pseudo-tetrahedral iridium-hydride complexes in proximity of a carbon dioxide and a water molecule which behaves as a proton-shuttle (see Figure 1 and Figure S1, Supporting Information). The two RCs are tautomers: in **RC_{NH}** the coordinated moiety is —CONH₂, in **RC_{CO}** is —C(OH)NH. The former is less stable than the latter by 4.5 kcal/mol in terms of Δ*G*.

The activation barrier for the process is lower for the NH path (Δ*G*[‡] = 8.5 kcal/mol with respect to the reactant complex **RC_{NH}**) than for the CO path (Δ*G*[‡] = 12.9 kcal/mol with respect to **RC_{CO}**) and the reaction is endothermic in both cases (Δ*G_{rxn}* = 4.2 kcal/mol for the CO path and Δ*G_{rxn}* = 1.1 kcal/mol for the NH path, for an analysis of the whole path, please see Menendez Rodriguez et al.¹⁴).

The two transition states (**TS_{NH}**) and (**TS_{CO}**) have very similar features (Figure 1 and Figure S1). **TS_{NH}** is a complex concerted transition state (it shows only one imaginary frequency of −640.8 cm^{−1}), in which i) the hydride transfers from the iridium center toward the electrophilic carbon atom of carbon dioxide (C¹H¹, *r_{C-H}* = 1.245 Å), ii)

the water molecule donates a proton to the oxygen atom of CO₂ (O¹H², *r_{O-H}* = 1.435 Å) and iii) the same water molecule abstracts a proton from the NH₂ moiety of the picolinamide ligand (O²—H³, *r_{O-H}* = 1.171 Å).

TS_{CO} is also concerted (it shows only one imaginary frequency of −143.3 cm^{−1}) and the involved chemical processes are similar to those described for **TS_{NH}**. The main difference is that water abstracts a proton from the —OH moiety of the ligand (O²H³). About the distances, i) for C¹H¹, *r_{C-H}* = 1.211 Å, ii) for O¹H², *r_{O-H}* = 1.449 Å and iii) for O²H³, *r_{O-H}* = 1.116 Å). A NBO analysis revealed that the main orbital interactions involved in this TS are: i) from σ(Ir—H) to π*(C¹O¹) and π*(C¹O²); ii) from lp(O¹) to σ*(O²H²); and iii) from lp(O²) to σ*(O³H³) (Table S1). For curly arrows pictures of **TS_{NH}** and **TS_{CO}**, see Figure S2.

In a three-body TS, the fragmentation choice cannot be unequivocal, but it depends on which chemical process one is interested in. In our case, the two interesting fragmentation schemes are [CO₂][−]·[Cp*IrH(picolin-amide)(H₂O)] (fragmentation scheme 1), if one is more interested in the hydride transfer from iridium to carbon dioxide or [H₂O][−]·[Cp*IrH(picolin-amide)(CO₂)] (fragmentation scheme 2), if the focus is on the proton transfer from the ligand to the water. The EDA results obviously depend on the fragmentation scheme: using the fragmentation scheme 1, *E_{int}* is −63.3 kcal/mol, composed of *E_{oi}* = −173.9, *E_{elst}* = −80.1 and *E_{Pauli}* = 196.5 kcal/mol, whereas by using the fragmentation scheme 2 the corresponding values are −54.5, −127.4, −54.5, and 140.1 kcal/mol, respectively (see also Tables S7 and S9).

Given the importance of the orbital stabilization, it is extremely interesting to further decompose Δ*E_{oi}*. The NOCV analysis has been applied to **TS_{CO}** (Figure 2). By fragmenting the TS according to fragmentation scheme 1, two relevant interactions can be disentangled and quantified: the formation of the hydride-CO₂ covalent bond (Δ*ρ*₁, blue region between C¹ and H¹) and the transfer of the proton from water to CO₂ (Δ*ρ*₂, blue region between O¹ and H²). The

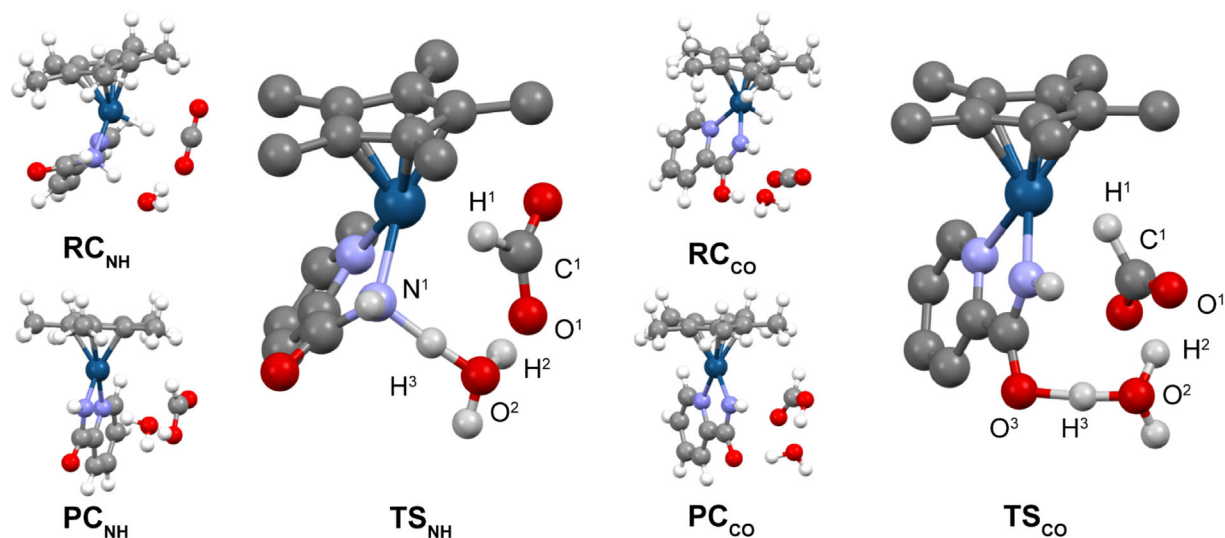


FIGURE 1 DFT-optimized geometries of **RC_{NH}**, **TS_{NH}**, and **PC_{NH}** (left) and **RC_{CO}**, **TS_{CO}** and **PC_{CO}** (right)

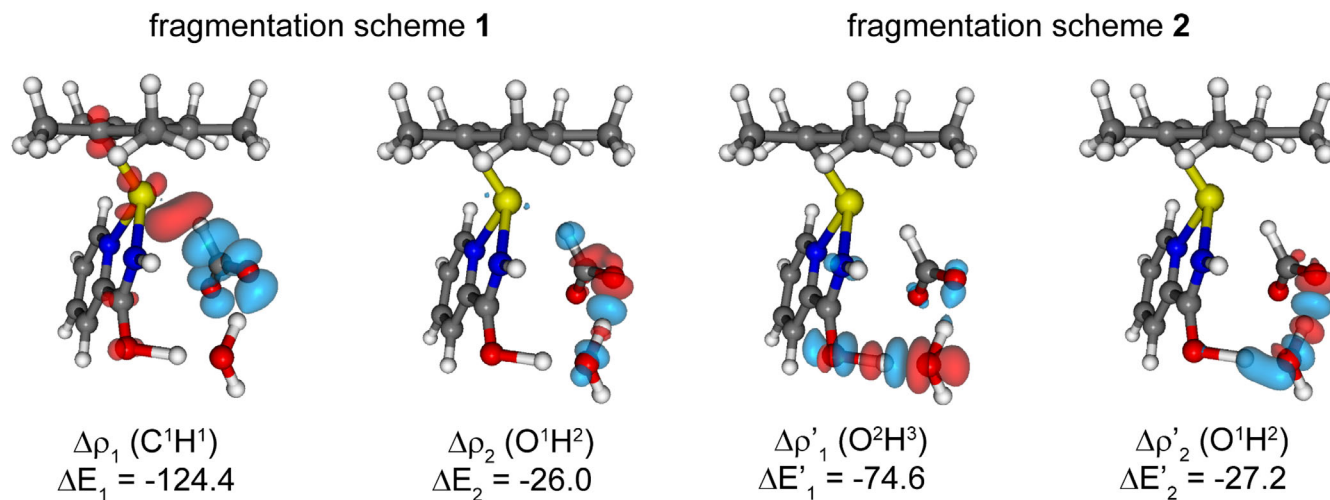


FIGURE 2 Isodensity surfaces (6 me a.u.⁻³) for the deformation maps relative to the $\Delta\rho_k$ ($k = 1-2$) contributions of the (left) $[\text{CO}_2] \cdots [\text{Cp}^*\text{IrH}(\text{picolin-amide})(\text{H}_2\text{O})]$ (fragmentation scheme 1) and (right) $[\text{H}_2\text{O}] \cdots [\text{Cp}^*\text{IrH}(\text{picolin-amide})(\text{CO}_2)]$ (fragmentation scheme 2) interactions for the TS_{CO} structure (the charge flux is red \rightarrow blue). For each NOCV, the corresponding orbital energy contributions ΔE_k are reported in kcal/mol

orbital energies associated to these interactions are ΔE_1 and ΔE_2 amounting to -124.4 and -26.0 kcal/mol (total $\Delta E_{\text{oi}} = -173.9$ kcal/mol), respectively. Other blue and red regions are coherent with the fragment polarization due to the incipient formation of the covalent bond.

On the other hand, by changing the fragmentation to scheme 2, the third relevant interaction can be singled out, which is the formation of the O^2H^3 bond ($\Delta E'_1$, -74.6 kcal/mol out of a total $\Delta E_{\text{oi}} = -127.4$ kcal/mol). Noteworthy, also within this fragmentation the O^1H^2 component can be isolated ($\Delta\rho'_2$). The Electron Density Deformation (EDD) map corresponding to $\Delta\rho_2$ and $\Delta\rho'_2$ are very similar, with some differences only in the polarization regions. This suggests us that the choice of the fragmentation scheme may be not crucial and, more importantly from our point of view, that the results of two different fragmentation schemes of the same geometry can be qualitatively compared and discussed together. The values of ΔE_2 and $\Delta E'_2$ are -26.0 and -27.2 kcal/mol, confirming the substantial equivalence between $\Delta\rho_2$ and $\Delta\rho'_2$ and indicating the robustness of the analysis. Anyway, this should be always verified, when possible.

The isolation of the three components is a very gratifying result and, despite the different $\Delta\rho_k$ values cannot be quantitatively compared, as they refer to different bonds, the picture that emerges clearly suggests that the hydride transfer from the metal is the key stabilizing step of the reaction.

In order to have a more detailed picture, we analyzed the path connecting **RC** to TS_{CO} to **PC**. There are different ways for this task. A particularly widespread method is the Intrinsic Reaction Coordinate (IRC),⁴² defined as the minimum energy reaction pathway (MERP) in mass-weighted cartesian coordinates between the transition state of a reaction and its reactants and products. Unfortunately, in our case the IRC method, as implemented in ADF, while it led to energy minima that match with RC_{CO} and PC_{CO} , it locates structures along the MERP

that are extremely close to TS_{CO} (Figure S3 and Tables S2–S3). In this way, we cannot have a global view of the reaction. We believe that this result depends on the high complexity of TS_{CO} , which lies in a very complex Potential Energy Surface (PES). The risks of the IRC method are known in literature,^{42,43} and Bickelhaupt and Houk in their review³⁹ write: “The IRC is a complex combination of geometry parameters, which complicates its interpretation.” The IRC method is probably the best choice for “simple” transition states, but it is less reliable in complex cases, as ours are (for the results and their discussion see Figure S3 and Tables S1 and S2 in this Supporting Information and discussion therein). In addition to this, the IRC procedure gives very little control on the critical factors that determine the output.

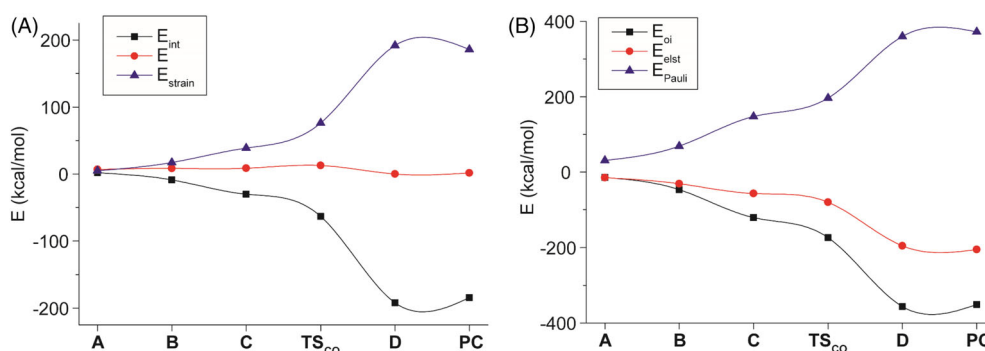
Therefore, we explored the Potential Energy Surface (PES) around the TS, through a series of partially constrained optimizations following wisely chosen geometrical parameters (Table 1). Actually, the choice of geometrical parameters is somehow “dictated” by the NOCV results (Figure 2). In our case, the most important contributions are the formation of the hydride transfer coordinate (i.e., the $\text{C}^1\text{—H}^1$ distance) and the proton abstraction (i.e., the $\text{O}^3\text{—H}^3$ distance). The result is something similar to a More O’Farrell-Jencks plot,^{44,45} and fits well with the chemical “common sense.”

Through the list of energies in Table 1, the minimum energy path connecting **RC** to **TS** to **PC** can be drawn (values highlighted in bold in Table 1). It is evident that the lowest energy path is not symmetrical and that the hydride transfer is by far the first molecular event, with the abstraction of the proton from the picolinamide moiety that becomes active only in the second part of the path. Representative geometries can be wisely chosen and extracted from the PES for NOCV analysis. Wise choices, in our opinion, are the geometry just before and after the **TS** (**C** and **D** in Table 1) and, depending on how much the **TS** is early (similar to **RC**) or late (similar to **PC**) other geometries homogeneously spread along the minimum energy path of the

TABLE 1 Relative energies (in kcal/mol, structure **D** as reference) of partially optimized geometries around TS_{CO}

$\text{C}^1\text{--H}^1$							
$\text{O}^3\text{--H}^3$	1.10	1.211	1.25	1.40	1.55	1.70	1.85
1.1	8.62		8.48 (C)	8.42	8.33 (B)	7.14	6.70 (A)
1.116		12.86 (TS)					
1.2	5.51		9.65	10.23	10.61	9.82	8.23
1.3	3.87		12.93	11.53	12.07	13.18	11.67
1.4	1.30		13.16	12.52	14.83	14.70	13.57
1.5	0.0 (D)		13.61	13.24	16.23	16.52	15.40

Note: Distances are in Å. Bold energies refer to the lowest energy path and representative geometries are labeled by a capital letter in parenthesis.

FIGURE 3 (A) Activation strain diagram for the Ir-catalyzed CO_2 activation (CO path); (B) decomposition of E_{int} in its components along the reaction coordinate

PES can be picked out. In the case of TS_{CO} , the TS is quite late, therefore more geometries are needed before the TS (A and B in Table 1). The procedure is completely customizable and if there is a region that is worth to be studied in detail, a higher local grid density can be used. By using an analogous scheme, similar results can be obtained for TS_{NH} (see Tables S5, S11 and S15 in the Supporting Information).

Now that A–D partial geometries are available, the entire path can be analyzed. Plotting the activation strain diagram and the EDA components (fragmentation scheme 1) with the reaction coordinate leads to the graphs shown in Figure 3. It appears clear that, the interaction energy is essential to compensate the high distortion penalty. In fact, given an activation energy of 12.9 kcal/mol, E_{strain} is 74.2 kcal/mol, mostly compensated by the interaction energy ($E_{\text{int}} = -61.2$ kcal/mol). By using a different fragmentation scheme (2, $[\text{H}_2\text{O}]\cdots[\text{Cp}^*\text{IrH}(\text{picolin-amide})(\text{CO}_2)]$), things are qualitatively similar (Tables S4 and S6, Supporting Information).

The ability of the ETS-NOCV approach of separating the main event occurring in the reaction (i.e., the iridium-to- CO_2 hydride transfer and the proton abstraction from water) remains unaltered along the reaction coordinate: as displayed in Figure S4 in the Supporting Information, the stabilizing interactions described at the TSs are still well-described along the reaction path.

Table 2 lists the orbital contributions for all the molecular events, either from fragmentation schemes 1 and 2 or both, showing that all of them increase as the reaction proceeds (formation of chemical bonds). As the absolute values cannot be directly compared, a normalization is necessary (see also Table S8).

For this reason, taking the values obtained from the PC complex as 100%, for each molecular event s (C^1H^1 , O^1H^2 and O^2H^3) the ratio.

$$\xi_s(j) = 100 * \Delta E_s^j / \Delta E_s^{\text{PC}} \quad (1)$$

with j going from A to PC, can be calculated and compared for the two paths (Figure 4). $\xi_s(j)$ represents the degree of completion for that step, again only from the orbital point of view.

For the O^1H^2 contribution, the fragmentation scheme 1 has been used for the plot but using the fragmentation scheme 2 would have led to a qualitatively similar trend. Only for the geometry C ΔE_2 and $\Delta E_2'$ are quite different. Obviously, in the case of a bond breaking, ΔE_k^{RC} could be taken as 100%.

Analogously to what derived from the analysis of Table 2, for the CO path the orbital contribution due to the hydride transfer rises from the beginning of the reaction, whereas the proton transfers O^1H^2 and O^2H^3 increase slowly in the first half of the reaction and undergo a steep rise in the correspondence of the TS. Here, the values of ξ for C^1H^1 , O^1H^2 , and O^2H^3 are 51%, 33%, and 39%, respectively. Interestingly, the two paths are sensibly different under this point of view, as in the NH path the interaction (which is a hydrogen bond that evolves to a covalent bond) between the water and CO_2 is much more important in the first part of the path. This can be related to the higher acidity of the amide with respect to an alcohol. In the CO path, the C^1H^1 bond is even shorter in the D structure than in PC (1.100 and 1.108 Å, respectively), explaining why $\xi_{\text{C}^1\text{H}^1}(\text{D}) > 100\%$. Similarly, for the NH path, O^2H^2 is 1.107 and 1.587 in structures D and PC, leading to a $\xi_{\text{O}^1\text{H}^2}(\text{D})$ of 125%.

TABLE 2 Orbital energy contributions (ΔE_k , in kcal/mol) associated to the three main contributions involved in **TS1_{CO}** (fragmentation scheme 1) values in parentheses refer to the corresponding $\Delta E'_k$ values for the O^1H^2 contribution (fragmentation scheme 2)

Geometry	C^1H^1	O^1H^2	O^2H^3
A	-8.3	-2.7 (-2.1)	-22.9
B	-32.7	-6.2 (-3.5)	-24.4
C	-88.9	-15.9 (-6.7)	-27.2
TS	-124.4	-26.0 (-27.2)	-74.6
D	-249.7	-75.0 (-93.8)	-150.1
PC	-242.3	-78.3 (-90.0)	-191.8

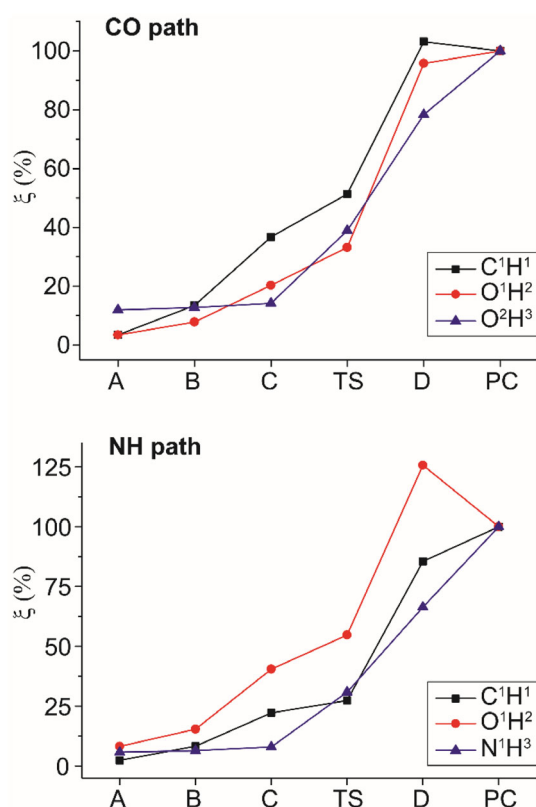


FIGURE 4 Trend of $\xi_s(j)$ with the reaction coordinate for the CO reaction paths

Substitution of one amidic proton with the electron-donating methoxy group is unfavorable for the reaction (the activation Gibbs' free energy becomes higher by 2.6 and 3.6 kcal/mol for the CO and NH path, respectively). Again, two different paths can be computed, passing through **TS_{NH_{OMe}}** and **TS_{CO_{OMe}}** and these two TSs are concerted, each with only one imaginary frequency (-90.8 and -683.3 cm^{-1} , respectively). Anyway, the normalized trends of ξ_s values are similar, suggesting that the mechanism remains substantially unaltered (Tables S10–S15, Supporting Information).

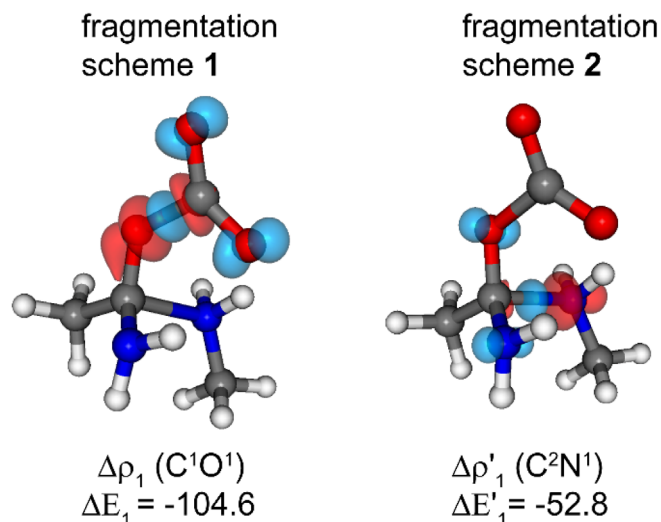


FIGURE 5 Isodensity surfaces (13 me a.u.^{-3}) for the deformation maps relative to the $\Delta\rho_1$ contribution of the (left) $[CO_2] \cdots [(CH_3CONH_2)(NH_2Me)]$ (fragmentation scheme 1) and (right) $[NH_2Me] \cdots [(CH_3CONH_2)(CO_2)]$ (fragmentation scheme 2) interactions for the **TS_{amide}** structure (the charge flux is red \rightarrow blue). For each NOCV, the corresponding orbital energy contributions ΔE_k are reported in kcal/mol

2.2 | CO_2 -promoted nucleophilic attack on an amide and similar reactions

The second interesting case is about the recently proposed interaction between an amide and CO_2 , which demonstrated to actively promote the transamidation reaction (Scheme 2).¹⁵

According to the experimental and theoretical mechanistic studies, the CO_2 acts as a template, using its acidic site to bind the oxygen of the ester, forming a carbonate, and the basic site to establish a strong H-bond with the attacking amine. In the subsequent step, the carbonate group acts as a proton shuttle, abstracting a proton from the attacking amine and transferring it to the nitrogen of the amide, therefore allowing the release of the leaving group with the simultaneous regeneration of CO_2 . According to the experimental results, almost all the amides receive an acceleration, but the best results are obtained with Weinrab amides (N-methoxy-N-methylamides), for which the activation energy is lower (experimental $\Delta H^\ddagger = 19.0$ kcal/mol, theoretical $\Delta H^\ddagger = 21.0$ kcal/mol). Anyway, a high temperature is generally required (around $80^\circ C$).¹⁵

For our model reaction (see Figure S5, Supporting Information), the concerted TS, **TS_{amide}** (see Figure 5), shows only one imaginary frequency (-307.3 cm^{-1}) in which there are the concurrent formation of a bond between the carbon of CO_2 and the oxygen of the amide ($C^1O^1 = 1.580$ Å) and the formation of the bond between the carbon of the amide and the nitrogen of the amine ($C^2N^1 = 1.924$ Å), leading to the tetrahedral intermediate **PC_{amide}**. The step is strongly endothermic ($\Delta G_{rxn} = 26.3$ kcal with respect to the reactant complex **RC_{amide}**, $\Delta G^\ddagger = 28.2$ kcal/mol), much less favored than with the Weinrab amide but still useful as a test case. Removing the carbon dioxide, **PC_{amide}** is

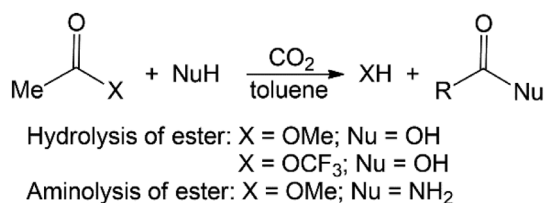
not a stable stationary point and decomposes back to the initial reactants. From the orbital point of view, the NBO analysis of TS_{amide} evidences the following orbital interactions: i) from $\text{lp}(\text{O}^1)$ to $\pi^*(\text{C}^1\text{O}^2)$ and $\pi^*(\text{C}^1\text{O}^3)$; ii) from $\text{lp}(\text{N}^1)$ to $\pi^*(\text{C}^2\text{O}^1)$; and iii) from $\text{lp}(\text{C}^1\text{O}^3)$ to $\sigma^*(\text{N}^1\text{H}^1)$ (Table S16). For the curly arrow picture, see Figure S7. It is important to remember that this step is not stand-alone, but the rate determining step of the entire reaction, therefore its analysis is justified.

We have applied the ETS-NOCV analysis in this case (Figure 5) and the two contributions can be effectively separated and quantified, ETS-NOCV as done above for the iridium complexes: indeed, by fragmenting TS_{amide} in $[\text{CO}_2] \cdots [(\text{CH}_3\text{CONH}_2)(\text{H}_2\text{NMe})]$ (fragmentation scheme 1, Figure 5), the C^1O^1 component has a $\Delta E_1 = -104.6$ kcal/mol (out of a total $\Delta E_{\text{oi}} = -137.1$ kcal/mol, see Figure 5 for the numbering of atoms), and, considering the same component in PC_{amide} (-159.2 kcal/mol), ξ can be calculated as 65%. On the other hand, by fragmenting TS_{amide} in $[(\text{CH}_3\text{CONH}_2)(\text{CO}_2)] \cdots [\text{H}_2\text{NMe}]$ (fragmentation scheme 2, Figure 5), the C^2N^1 component in TS_{amide} is $\Delta E'_1 = -52.8$ kcal/mol ($\xi = 30\%$, total $\Delta E_{\text{oi}} = -63.1$ kcal/mol), revealing that the interaction of CO_2 with the amide is indeed the most stabilizing molecular event that facilitates the whole reaction. In this case, the abstraction of the N^1H^1 occurs in the second step of the reaction (Figure S6, Supporting Information).

Based on the above picture, it is possible to theoretically study similar reactions, such as the hydrolysis or aminolysis of an ester (Scheme 3 and Figure 6) with our strategy, in order to quantify the impact of such chemical variations on the $\xi_{s(j)}$ values.

The corresponding energy profiles can be found in the Supporting Information (Figures S9–S11 and Tables S17–S28). In the hydrolysis of esters, the model case $\text{H}_2\text{O} + \text{MeCOOMe}$ has been studied. The TS (TS_{hydro}) shows only one imaginary frequency (-506.2 cm^{-1}) in which three molecular events are clearly visible: not only the formation of the C^1O^1 bond and the formation of a bond between the oxygen of the water and the carbon of the amide (C^2O^2) (equivalent to the C^2N^1 bond in the trans- amidation), but also the proton transfer from the water to CO_2 (O^3H^1) takes place at the same time (Figure 7).

Also in this case involving three concerted molecular events, the NOCV analysis succeeds in perfectly decomposing all the contributions, using two different fragmentation schemes. As in the iridium case, the proton transfer O^3H^1 can be isolated using both the schemes, with similar EDD plots (Figure 7) and a difference of some units of kcal/mol in the orbital contributions.



SCHEME 3 Chemical variations on the CO_2 -promoted trans- amidation reaction

For the hydrolysis of a fluorinated ester, MeCOOCF_3 , and the aminolysis of an ester, $\text{NH}_3 + \text{MeCOOMe}$, the framework is similar and, in both cases, the three components can be decomposed.

In order to extract intermediate geometries along the PES, the IRC approach as implemented in ORCA has been used, but the results are again limited and unsatisfactory, even if the procedure is generally fast. Indeed, for the trans- amidation reaction, the IRC leads to two structures with C^2N^1 distances 1.991 and 1.789 Å, whereas through the exploration of the PES around TS_{amide} the structures with C^2N^1 distances from 2.1 Å (A geometry) to 1.6 Å (D geometry) can be isolated, allowing a more thorough study of the reaction step (Figure S5). For the hydration of an ester, the IRC procedure is able to cover a larger portion of the PES and provide acceptable intermediate geometries, but here we will use the PES procedure in all the cases. On the other hand, it must be said that the ξ values are generally in qualitative agreement between the two methods (Tables S19, S22, S25, and S28). In general, the PES procedure is a good alternative when the IRC one fails or more control is needed.

Figure 8 sums up the results of the NOCV analysis along the different reaction coordinates. The trends are quite different in the details, despite the general similarities between the TSs geometries. In particular, it can be appreciated and quantified how the nucleophilic

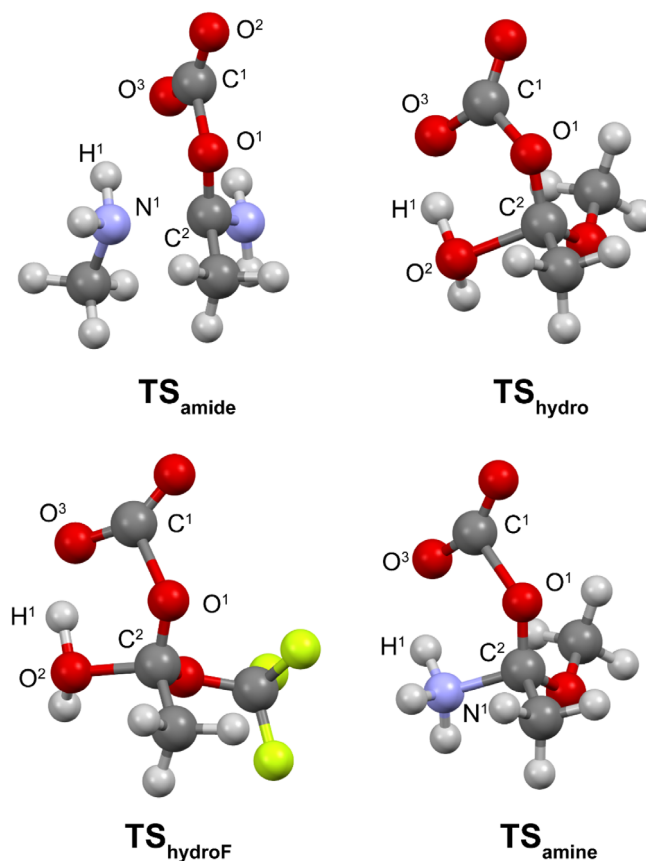


FIGURE 6 DFT-optimized TS for the reactions of trans- amidation, hydrolysis of two different esters and aminolysis of an ester

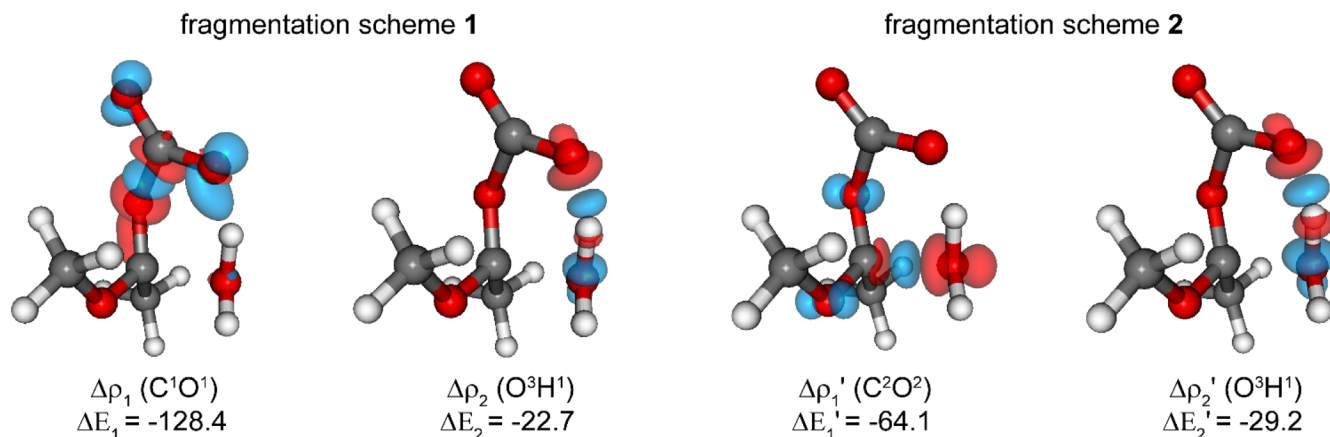
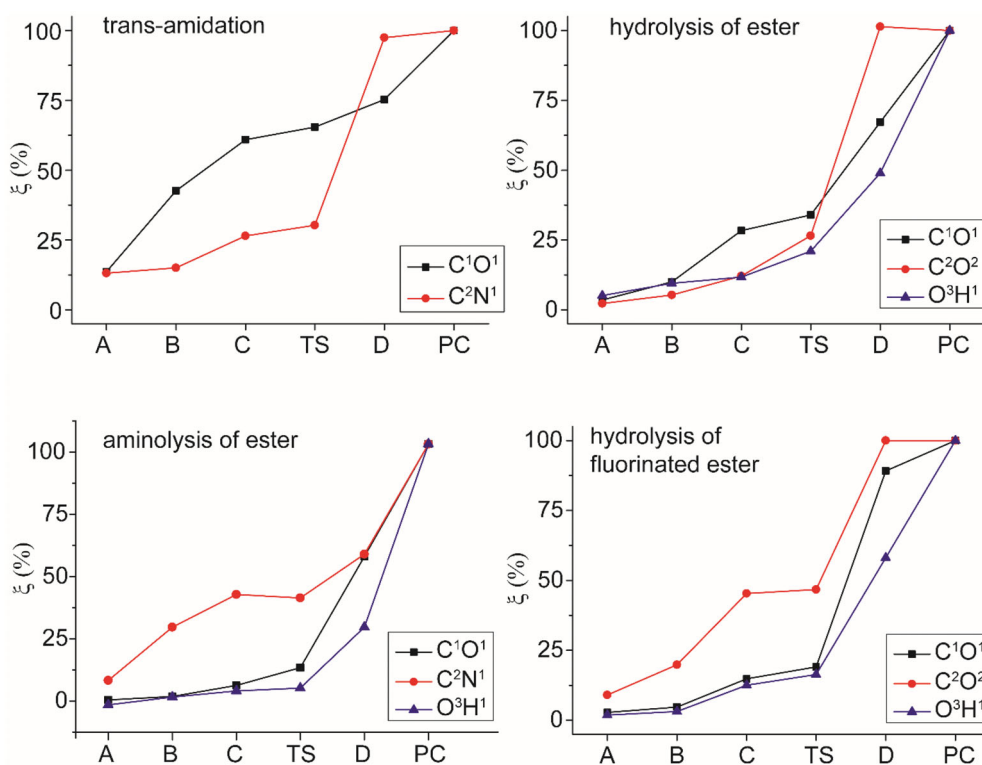


FIGURE 7 Isodensity surfaces (13 me a.u.⁻³) for the deformation maps relative to the $\Delta\rho_k$ ($k = 1-2$) contributions of the (left) [CO₂]⁻⋯[(CH₃COOCH₃)(H₂O)] and (right) [H₂O]⁻⋯[(CH₃COOCH₃)(CO₂)] interactions for the TS_{hydro} structure (the charge flux is red → blue). For each NOCV, the corresponding orbital energy contributions ΔE_k are reported in kcal/mol



attack (red dots in Figure 8) becomes the prevalent step by making the ester more acidic (fluorinated substituents) or the nucleophile stronger (ammonia instead of water).

For **TS_{amide}**, $\xi_{C1O1} = 65\%$ and $\xi_{C2N1} = 30\%$, as said, the formation of the carbonate moiety is by far the first and more advanced process during the concerted step. For **TS_{hydro}**, $\xi_{C1O1} = 34\%$, whereas $\xi_{C2O2} = 26\%$ and $\xi_{O3H1} = 21\%$, suggesting that the formation of the bond with the CO₂ is still the more advanced process, but to a much smaller degree with respect to the nucleophilic attack (TS “early”). Similarly, the proton transfer from water to the CO₂/carbonate moiety is almost as important as the other two steps.

For **TS_{amine}**, $\xi_{C2N1} = 42\%$, whereas $\xi_{C1O1} = 15\%$ and $\xi_{O3H1} = 8\%$, indicating that the nucleophilic attack becomes the most advanced process because of the higher nucleophilicity of ammonia with respect to water, whereas the proton transfer is by far the least important, given the reduced acidity of the ammonium with respect to the hydronium ion.

Finally, for **TS_{hydroF}**, $\xi_{C1O1} = 19\%$, whereas $\xi_{C2O2} = 47\%$ and $\xi_{O3H1} = 16\%$, suggesting that the nucleophilic attack is again the most advanced process of the concerted step, but for a different reason than in the case of **TS_{amino}**. In this case the fluorine makes the ester carbon more electrophilic, driving the other two steps of the reaction.

It can be appreciated the level of detail of this characterization of concerted TSs, quantifying concepts that can be qualitatively obvious or intuitive and paving the way to a new method to optimize catalysts and reaction paths. For the organic reactions the similarity with the More O'Farrell-Jencks (MOJ) plots^{44,45} is even more evident (Figure S8 and Table S29) and the two plots show a substantial agreement. A systematic difference exists between the two analysis, as orbital percentages are always smaller than bond orders one.

Before concluding it may be interesting to compare the results of our analysis with information that can be extracted by considering solely the molecular structures along the minimum energy path. For convenience, we can define the normalized distances for each molecular event s as

$$r'_s(j) = 100 * \left[1 - \left(\frac{r_s^j - r_s^{\text{PC}}}{r_s^{\text{PC}}} \right) \right] \quad (2)$$

with j going from A to PC. It must be said that in the case of TSs containing only two molecular events, the trends of ξ_s and r'_s are quite similar (as for TS_{amide} see Figure S12, Supporting Information), whereas in the case of more than two molecular events, the trends are quite different (as for TS_{hydro}, see Figure S13, Supporting Information), especially for the molecular distance that is not constrained in the construction of the non-stationary points. Of course, ξ_s refers only to the orbital contribution (which is however, the component of the interaction which is expected to be more sensitive to the chemical modulation effects), whereas r'_s , apart all the considerations about its reliability, is likely related to the sum of all the components, but exactly for this reason the comparison is interesting.

3 | CONCLUSION

In conclusion, we have shown here that an extensive ETS-NOCV analysis (also combined with ASM and EDA approaches) along a selected cut of the potential energy surface around the TS structure is able to give precious insights about CO₂-related concerted transition states. This is mainly due to the fact that the acidic and basic sites of CO₂ establish orthogonal interactions that can be easily separated by this methodology. Therefore, the relative importance of each “molecular event” that is interlaced in the concerted mechanism becomes accessible in a more quantitative manner.

Importantly, as the widespread IRC procedure did not give satisfactory results for our complex TSs, we explored the PES through a series of partially optimized geometries, using the ETS-NOCV analysis of the TS to choose the geometrical parameters to follow.

The examples illustrated here are quite different from each other, with the exact purpose to test the ETS-NOCV methodology in very different scenarios: the synthesis of formic acid from a hydrogenated iridium complex (or the decomposition of formic acid, as in the original paper) and the quite innovative use of CO₂ as a catalyst in the transamidation reaction and its chemical variants (amino- and hydrolysis of an ester). In both cases, the ETS-NOCV analysis along a selected cut

of the PES around TS allowed the separation of the key chemical events involved in the concerted step, quantifying their contribution to the total orbital interaction and allowing to quantify the advancement of each of them along the reaction path, either at the transition state and in any other point of the reaction coordinate (non-stationary points). Indeed, the methodology proposed here is able to disentangle in a quantitative manner the interactions related to different “molecular events” not only at the transition state, but also exploring the lowest energy path around the latter, thus enabling a control on the variable predominance of each component along the reaction path.

Applying the proposed scheme ETS-NOCV to the chemical variants of transamidation (hydro- and aminolysis of esters) revealed that the effect of a substitution or the change of a reactant can be rationalized and quantified in detail.

This approach has yet to be tested in other kind of reactions but promises to be effective approach for the detailed characterization of concerted TSs. Even more importantly, it is a potential tool for more rational optimization of a catalyst, whose utility and effectiveness will be tested in the near future.

4 | COMPUTATIONAL DETAILS

Geometry optimization. Organometallic species have been optimized using ADF 2014.09,^{46,47} with the BP86 functional, the TZ2P basis set, the scalar ZORA Hamiltonian for relativistic effects. Dispersion was introduced with the D3 correction proposed by Grimme²⁷ with the Becke-Johnson (BJ) damping scheme²⁸ and the solvent (water) was included with the COSMO model.⁴⁸ This computational setup has been proven to be very accurate in describing catalysis by iridium-containing organometallic systems in benchmark calculations.⁴⁹ For organic species, ORCA 4.1.0⁵⁰ has been used, with the B3LYP functional, def2/J auxiliary basis set, RIJCOSX approximation and the def2-tzvp basis set. Dispersion was introduced with the D3-BJ scheme and the solvent (toluene) was included with the CPCM model. ORCA has been chosen because ADF is notoriously computationally demanding with B3LYP functional. It is important to underline that the results of organic and organometallic systems are never directly compared, therefore we do not need concordance of computational details and each system can be treated with specifically chosen computational details. Anyway, we compared the variation of EDA results with the code and computational details used (Tables S30–S32, Supporting Information). It can be seen that both variables have a small effect on EDA results, not higher than some kcal/mol.

The IRC run for TS_{CO} has been carried out with the same computational protocol used for the other analyses (BP86-D3(BJ)/TZ2P/SR-ZORA and COSMO for solvent (water) effects) using a more recent version of the ADF software (AMS 2020.104) with default options (100 maximum IRC points, 0.001 eh/Å gradient convergence and step size of 0.2 (amu)^{1/2} bohr) and the exact hessian calculated from a previous analytical frequencies calculation. For organic species, the IRC run has been carried out using ORCA 4.1.0 at the same theory level used for optimization.

All stationary points have been characterized by verifying the presence of no imaginary frequencies (intermediate species) or one imaginary frequency (transition states) coherently with the reaction coordinate.

NBO analyses have been performed using the NBO 7.0 suite of software.⁵¹

*Energy decomposition analysis.*¹⁶ The EDA has been performed with a large variety of functional/basis sets combinations, either using ORCA 4.1.0 or ADF 2014.09.⁴⁶ The EDA allows the decomposition of the bond energy into physically meaningful contributions. The interaction energy (E_{int}) is the difference of energy between the adduct and the unrelaxed fragments. It can be divided into contributions associated with the orbital, steric and dispersion interactions, as shown in Equation (3).

$$\Delta E_{\text{int}} = \Delta E_{\text{st}} + \Delta E_{\text{oi}} + \Delta E_{\text{disp}} \quad (3)$$

ΔE_{st} is usually called the steric interaction energy and it is the sum of ΔE_{elst} , the classical electrostatic interaction between the unperturbed charge distributions of the fragments (ρ_A and ρ_B) at their final positions in the adduct, and the Pauli repulsion (ΔE_{Pauli}) that is the energy change associated with going from $\rho_A + \rho_B$ to the antisymmetrized and renormalized wave function. The decomposition of ΔE_{st} is not possible with ORCA 4.1.0, while it is with ADF. ΔE_{oi} is the contribution arising from allowing the wave function to relax to the fully converged one, accounting for electron pair bonding, charge transfer and polarization, while ΔE_{disp} is the contribution of the dispersion forces and it is available only when a specific dispersion correction is used.

*Extended Transition State-Natural Orbitals for Chemical Valence (ETS-NOCV) analysis.*¹⁸ In the ETS-NOCV approach, the electron density rearrangement taking place upon formation of AB from fragments A and B is defined with respect to a reference system made up of the occupied ψ_i^A and ψ_i^B orbitals of A and B orthonormalized with respect to each other (ψ_i^0). In other words, rather than two separate A and B determinants, their antisymmetrized product is taken as the fragment–fragment non-interacting reference (the so-called “promolecule”). The resulting electron density rearrangement,

$$\Delta \rho_{\text{tot}} = \sum_i |\psi_i^{AB}|^2 - |\psi_i^0|^2 \quad (4)$$

where $\psi_i^{(AB)}$ is the set of occupied orbitals of the adduct, can be brought into diagonal form in terms of NOCVs. These are defined as the eigenfunctions, $\phi_{\pm k}$, of the so-called “valence operator”:^{52–54}

$$\hat{V} = \sum_i \left(|\psi_i^{(AB)}\rangle \langle \psi_i^{(AB)}| - |\psi_i^0\rangle \langle \psi_i^0| \right) \quad (5)$$

The fragmentation depends on the interaction under examination and is generally indicated in each case. The NOCVs can be grouped in pairs of complementary orbitals (ϕ_k, ϕ_{-k}) corresponding to eigenvalues with same absolute value but opposite sign (Equation (6)).

$$\hat{V} \phi_{\pm k} = \pm \nu_k \phi_{\pm k} (\nu_k > 0) \quad (6)$$

where k numbers the NOCV pairs ($k = 0$ for the largest value of $|\nu_k|$). In this framework, $\Delta \rho_{\text{tot}}$ can be defined as in Equation (7).

$$\Delta \rho_{\text{tot}} = \sum_k \nu_k \quad (7)$$

Hence, on formation of AB from the promolecule, a fraction ν_k of electrons is transferred from the ϕ_{-k} to the ϕ_k orbital. Only some NOCVs pairs have ν_k significantly different from zero and this subgroup is generally enough to describe the A···B interaction. For each value of k , an energy contribution associated with the k -th NOCV pair is given.

The ETS-NOCV analysis has been performed with ORCA 4.1.0 for organic molecules and ADF2014.09 for organometallic systems.

4.1 | Activation Strain Model

The Activation Strain Model (ASM)^{38–40} is a popular approach often used in order to get insights into the factors that control the activation barrier of a chemical reaction. For a process connecting a reactant complex (RC) and a transition state (TS), the electronic activation barrier (ΔE^\ddagger) can be in general decomposed as follows:

$$\Delta E^\ddagger = \left[\Delta E_{\text{strain}}^{\text{TS}} - \Delta E_{\text{strain}}^{\text{RC}} \right] + \left[\Delta E_{\text{int}}^{\text{TS}} - \Delta E_{\text{int}}^{\text{RC}} \right] = E_{\text{strain}} + E_{\text{int}} \quad (8)$$

where the “ $\Delta E_{\text{strain}}^{\text{TS}}$ ” and “ $\Delta E_{\text{strain}}^{\text{RC}}$ ” terms represent the energy penalty due to the distortion of the separated fragments constrained in the structures of TS and RC, respectively, whereas “ $\Delta E_{\text{int}}^{\text{TS}}$ ” and “ $\Delta E_{\text{int}}^{\text{RC}}$ ” represent the interaction energies between the fragments (with the geometries constrained at the ones assumed in the TS and RC, respectively) in the two structures. These terms can be grouped in the “ E_{strain} ” and “ E_{int} ” terms, that represent the overall distortion and interaction contributions to the activation barrier, respectively.

ACKNOWLEDGEMENTS

G.C. thanks University of Pisa for the support and Dr. Elisa Rossi for helpful discussions. Open Access Funding provided by Università degli Studi di Pisa within the CRUI-CARE Agreement.

CONFLICT OF INTEREST

The authors declare no potential conflict of interest.

DATA AVAILABILITY STATEMENT

All the original data are available on request from the authors.

ORCID

Gianluca Ciancaleoni  <https://orcid.org/0000-0001-5113-2351>

REFERENCES

- [1] Webpage, <https://gml.noaa.gov/ccgg/trends/monthly.html>.
- [2] J. Sekera, A. Lichtenberger, *Biophys. Econ. Sustain.* **2020**, *5*, 14.
- [3] H. A. Patel, J. Byun, C. T. Yavuz, *ChemSusChem* **2017**, *10*, 1303.
- [4] Ž. Kovačić, B. Likozar, M. Huš, *ACS Catal.* **2020**, *10*, 14984. <https://doi.org/10.1021/acscatal.0c02557>
- [5] M. W. Chase Jr., *J. Phys. Chem. Ref. Data Monogr.* **1998**, *9*, 1. <https://www.nist.gov/srd/journal-physical-and-chemical-reference-data-monographs-or-supplements>
- [6] H. A. Lara-García, B. Landeros-Rivera, E. González-Zamora, J. Aguilar-Pliego, A. Gómez-Cortés, A. Martínez, R. Vargas, G. Díaz, I. A. Ibarra, *Dalt. Trans.* **2019**, *48*, 8611.
- [7] X. Zhu, Y. Lu, C. Peng, J. Hu, H. Liu, Y. Hu, *J. Phys. Chem. B* **2011**, *115*, 3949.
- [8] D. W. Stephan, G. Erker, *Chem. Sci.* **2014**, *5*, 2625. <https://pubs.rsc.org/en/content/articlelanding/2014/sc/c4sc00395k/unauth>.
- [9] L. Liu, B. Lukose, B. Ensing, *ACS Catal.* **2018**, *8*, 3376. <https://pubs.acs.org/doi/10.1021/acscatal.7b04072>.
- [10] M. T. Nguyen, M. H. Matus, V. E. Jackson, V. T. Ngan, J. R. Rostad, D. A. Dixon, *J. Phys. Chem. A* **2008**, *112*, 10386.
- [11] X. H. Li, S. J. Ren, X. G. Wei, Y. Zeng, G. W. Gao, Y. Ren, J. Zhu, K. C. Lau, W. K. Li, *J. Phys. Chem. A* **2014**, *118*, 3503.
- [12] F. J. Fernández-Alvarez, A. M. Aitani, L. A. Oro, *Catal. Sci. Technol.* **2014**, *4*, 611.
- [13] R. Parida, S. Giri, *J. Mol. Model.* **2019**, *25*, 334.
- [14] G. Menendez Rodriguez, F. Zaccaria, L. Tensi, C. Zuccaccia, P. Belanzoni, A. Macchioni, *Chem. – A Eur. J.* **2021**, *27*, 2050.
- [15] Y. Yang, J. Liu, F. S. Kamounah, G. Ciancaleoni, J. W. Lee, *J. Org. Chem.* **2021**, *86*, 16867.
- [16] M. von Hopffgarten, G. Frenking, *Wiley Interdiscip. Rev. Comput. Mol. Sci.* **2012**, *2*, 43.
- [17] L. Zhao, M. von Hopffgarten, D. M. Andrada, G. Frenking, *Wiley Interdiscip. Rev. Comput. Mol. Sci.* **2018**, *8*, e1345. <https://doi.org/10.1002/wcms.1345>
- [18] M. P. Mitoraj, A. Michalak, T. Ziegler, *J. Chem. Theory Comput.* **2009**, *5*, 962.
- [19] M. Srebro, A. Michalak, *Inorg. Chem.* **2009**, *48*, 5361.
- [20] M. Mitoraj, A. Michalak, *J. Mol. Model.* **2007**, *13*, 347.
- [21] P. L. Bora, M. Novák, J. Novotný, C. Foroutan-Nejad, R. Marek, *Chem. – A Eur. J.* **2017**, *23*, 7315.
- [22] M. Novák, C. Foroutan-Nejad, R. Marek, *Phys. Chem. Chem. Phys.* **2015**, *17*, 6440.
- [23] G. Ciancaleoni, L. Belpassi, *J. Comput. Chem.* **2020**, *41*, 1185.
- [24] E. Buttarazzi, F. Rosi, G. Ciancaleoni, *Phys. Chem. Chem. Phys.* **2019**, *21*, 20478.
- [25] G. Marrazzini, C. Gabbiani, G. Ciancaleoni, *ACS Omega* **2019**, *4*, 1344.
- [26] G. Ciancaleoni, L. Belpassi, F. Marchetti, *Inorg. Chem.* **2017**, *56*, 11266.
- [27] G. Ciancaleoni, L. Rocchigiani, *Inorg. Chem.* **2021**, *60*, 4683.
- [28] S. Díaz, M. Z. Brela, S. Gutiérrez-Oliva, A. Toro-Labbé, A. Michalak, *J. Comput. Chem.* **2017**, *38*, 2076.
- [29] A. Roznowska, K. Dyduch, B. Y. Lee, A. Michalak, *J. Mol. Model.* **2020**, *26*, 1.
- [30] M. A. Van Bochove, M. Swart, F. M. Bickelhaupt, *J. Am. Chem. Soc.* **2006**, *128*, 10738.
- [31] D. Sorbelli, L. Belpassi, P. Belanzoni, *J. Am. Chem. Soc.* **2021**, *143*, 14433.
- [32] A. Artigas, I. Fernández, M. Solà, *J. Org. Chem.* **2019**, *84*, 9017.
- [33] D. Yepes, P. Jaque, I. Fernández, *Chem. – A Eur. J.* **2016**, *22*, 18801.
- [34] P. Vermeeren, T. A. Hamlin, F. M. Bickelhaupt, I. Fernández, *Chem. – A Eur. J.* **2021**, *27*, 5180.
- [35] I. Cortés, J. J. Cabrera-Trujillo, I. Fernández, *ACS Org. Inorg. Au.* **2022**, *2*, 44. <https://doi.org/10.1021/acscorginorgau.1c00023>
- [36] S. T. A. Hamlin, I. Fernández, P. Vermeeren, T. A. Hamlin, I. Fernández, F. Fernández, F. M. Bickelhaupt, *Chem. Sci.* **2020**, *11*, 8105.
- [37] P. Talaga, M. Z. Brela, A. Michalak, *J. Mol. Model.* **2018**, *24*, 27.
- [38] P. Vermeeren, S. C. C. van der Lubbe, C. Fonseca Guerra, F. M. Bickelhaupt, T. A. Hamlin, *Nat. Protoc.* **2020**, *15*, 649.
- [39] F. M. Bickelhaupt, K. N. Houk, *Angew. Chem. Int. Ed.* **2017**, *56*, 10070.
- [40] I. Fernández, F. M. Bickelhaupt, *Chem. Soc. Rev.* **2014**, *43*, 4953.
- [41] L. P. Wolters, F. M. Bickelhaupt, *Wiley Interdiscip. Rev. Comput. Mol. Sci.* **2015**, *5*, 324.
- [42] S. Maeda, Y. Harabuchi, Y. Ono, T. Taketsugu, K. Morokuma, *Int. J. Quantum Chem.* **2015**, *115*, 258.
- [43] W. J. Van Zeist, A. H. Koers, L. P. Wolters, F. M. Bickelhaupt, *J. Chem. Theory Comput.* **2008**, *4*, 920.
- [44] W. P. Jencks, *Chem. Rev.* **1972**, *72*, 705.
- [45] R. A. More O'Ferrall, *J. Chem. Soc. B Phys. Org.* **1970**, 274. <https://doi.org/10.1039/j29700000274>
- [46] G. te Velde, F. M. Bickelhaupt, E. J. Baerends, C. Fonseca Guerra, S. J. A. van Gisbergen, J. G. Snijders, T. Ziegler, *J. Comput. Chem.* **2001**, *22*, 931.
- [47] M. Swart, F. M. Bickelhaupt, *J. Comput. Chem.* **2008**, *29*, 724.
- [48] C. C. Pye, T. Ziegler, *Theor. Chem. Acc.* **1999**, *101*, 396.
- [49] A. Kazaryan, E. J. Baerends, *J. Comput. Chem.* **2013**, *34*, 870.
- [50] F. Neese, F. Wennmohs, U. Becker, C. Riplinger, *J. Chem. Phys.* **2020**, *152*, 224108. <https://doi.org/10.1063/5.0004608>
- [51] E. D. Glendening, J. K. Badenhop, A. E. Reed, J. E. Carpenter, J. A. Bohmann, C. M. Morales, C. R. Landis, F. Weinhold, NBO 6, Theoretical Chemistry Institute, University of Wisconsin, Madison, WI **2013**. <http://nbo6.chem.wisc.edu/>
- [52] R. F. Nalewajski, J. Mrozek, A. Michalak, *Int. J. Quantum Chem.* **1997**, *61*, 589.
- [53] R. F. Nalewajski, J. Ozek, *Int. J. Quantum Chem.* **1994**, *51*, 187.
- [54] R. F. Nalewajski, A. M. Köster, K. Jug, *Theor. Chim. Acta* **1993**, *85*, 463.

SUPPORTING INFORMATION

Additional supporting information may be found in the online version of the article at the publisher's website.

How to cite this article: D. Sorbelli, P. Belanzoni, L. Belpassi, J.-W. Lee, G. Ciancaleoni, *J. Comput. Chem.* **2022**, *43*(10), 717. <https://doi.org/10.1002/jcc.26829>